Cross-subject variability of the optic radiation anatomy in a cohort of 1065 healthy subjects

B. Herlin, I. Uszynski, M. Chauvel, C. Poupon, S. Dupont

Title :

Cross-subject variability of the optic radiation anatomy in a cohort of 1065 healthy subjects

Authors :

B. Herlin[1,2,3], I. Uszynski[1], M. Chauvel[1], C. Poupon[1], S. Dupont[2,3].

1: BAOBAB, NeuroSpin, Université Paris-Saclay, CNRS, CEA, Gif-sur-Yvette, France
2: AP-HP, Epilepsy Unit, GH Pitié-Salpêtrière-Charles Foix, 47-83 Boulevard de l'Hôpital, 75013, Paris, France.
3: Sorbonne Université, Paris, France

Corresponding author: B. Herlin (bastien.herlin@aphp.fr)

Author contribution:

B. Herlin: Protocol/project development, Data collection or management, Data analysis, Manuscript writing
I. Uszynski: Protocol/project development, Data management, Data Analysis, Manuscript writing/editing
M. Chauvel: Protocol/project development, Data analysis
C. Poupon : Protocol/project development, Manuscript writing/editing
S. Dupont: Protocol/project development, Manuscript writing/editing

Abstract

Introduction: Optic radiations are tracts of particular interest for neurosurgery, especially for temporal lobe resection, because their lesion is responsible for visual field defects. However, histological and MRI studies found a high inter-subject variability of the optic radiation anatomy, especially for their most rostral extent inside the Meyer's temporal loop. We aimed to better assess inter-subject anatomical variability of the optic radiations, in order to help to reduce the risk of postoperative visual field deficiencies.
Methods: Using an advanced analysis pipeline relying on a whole-brain probabilistic tractography and fiber clustering, we processed the diffusion MRI data of the 1065 subjects of the HCP cohort. After registration in a common space, a cross-subject clustering on the whole cohort was performed to reconstruct the reference optic radiation bundle, from which all optic radiations were segmented on an individual scale.
Results: We found a median distance between the rostral tip of the temporal pole and the rostral tip of the optic radiation of 29.2 mm (standard deviation: 2.1 mm) for the right side and 28.8 mm (standard deviation: 2.3 mm) for the left side. The difference between both hemispheres was statistically significant ($p=1.10^{-8}$).
Conclusion: We demonstrated inter-individual variability of the anatomy of the optic radiations on a large-scale study, especially their rostral extension. In order to better guide neurosurgical procedures, we built a MNI-based reference atlas of the optic radiations that can be used for fast optic radiation reconstruction from any individual diffusion MRI tractography.

Keywords :

Neuroanatomy, Magnetic Resonance Imaging, Tractography, White Matter, Optic Radiation

Statements and declaration :

This research has received funding from the European Union's Horizon 2020 Framework Program for Research and Innovation under the specific Grant No. 945539 (Human Brain Project SGA3).
Authors disclose no other financial or non-financial interests that could be directly or indirectly related to the work submitted for publication

Acknowledgement

Data were provided by the Human Connectome Project, WU-Minn Consortium (Principal Investigators: David Van Essen and Kamil Ugurbil; 1U54MH091657) funded by the 16 NIH Institutes and Centers that support the NIH Blueprint for Neuroscience Research; and by the McDonnell Center for Systems Neuroscience at Washington University.
This research has received funding from the European Union's Horizon 2020 Framework Program for Research

and Innovation under the specific Grant No. 945539 (Human Brain Project SGA3).

Introduction

Optic radiation's initial anatomical description originates from the French neuroanatomist Louis-Pierre Gratiolet, who described those tracts from their origin from the lateral geniculate body to their termination around the calcarine sulcus. The anatomical knowledge was then reinforced by other post-mortem studies, including Flechsig in 1896 and Meyer in 1907 who described their most rostral part within the temporal lobe, actually known as the “Meyer temporal loop”. This rostral part is the most vulnerable part of the optic radiations, and is particularly vulnerable to temporal lobe lesions or temporal excisions. When damaged, the rostral optic radiation bundle interruption results in a specific visual field defect: a superior homonymous quadrantanopia. This tract has been shown to have a high inter-subject variability in dissection studies performed in small cohorts of subjects [5, 26, 28], especially regarding its rostral extension within the temporal lobe. Knowledge of this individual variability of the optic pathways is crucial but cannot yet be determined by autopsy studies which are necessarily limited in the number of subjects studied.

Postoperative visual field defect remains frequent after temporal lobe surgery, concerning 15 to 50 % patients after a mesial temporal resection in patients with drug resistant epilepsy, related to an hippocampal sclerosis for most of them [16, 22, 27]. Visual field defect has been more frequently reported after left-sided surgery [16], suggesting a possible left-right difference in temporal loop extent. Nowadays, *in vivo* studies of brain white matter fiber tracts are possible thanks to diffusion MRI, which enables the estimation of the fiber direction in each voxel and the reconstruction of the white matter tracts using tractography algorithms. Fiber tractography might be used to better plan the surgical extent and thus reduce the visual field defect risk [34], since surgery seems more efficient when an intraoperative visualization is available [38]. However, the actual use of pre-operative optic radiation tractography is still limited by different parameters which make the comparison between studies difficult: i) the differences in hardware MRI systems ii) the tractography algorithms and iii) the sample size of the studies. Due to these limitations, diffusion MRI tractography, when used, still fails to avoid postoperative quadrantanopia in around 25% of patients undergoing medial temporal lobe surgery.

In this study, we used a probabilistic tractography method in a large cohort of 1065 healthy subjects to better assess inter-subject anatomical variability of the optic radiations and more specifically improve the anatomical knowledge of the temporal loop and better assess the potential inter-hemispheric variability. For this, we built a reference optic radiation bundle registered in the MNI template space, which can be used for fast optic radiation reconstruction from any diffusion MRI tractography in order to guide neurosurgical procedures and reduce the risk of postoperative visual field defect.

Methods

Database

We used the brain MRI dataset from the Human Connectome Project (Q1-Q4 release, 2015) acquired by Washington University in Saint Louis and University of Minnesota [39]. This database includes 1065 healthy subjects aged from 22 to 35 years, who all underwent an anatomical T1-weighted (T1w) with a 0.7mm spatial isotropic resolution and series of diffusion MRI (dMRI) scans using 3 different b-values of 1000, 2000, and 3000 s/mm2 and 90 diffusion directions per b-value shell, with a 1.25mm spatial isotropic resolution, conducted on a 3T MRI scanner. The data were already preprocessed and corrected for eddy current and susceptibility artifacts.

Individual subject analysis

We designed an analysis pipeline for processing the dMRI data, based on the Ginkgo toolbox developed by the CEA/NeuroSpin team freely available at https://framagit.org/cpoupon/gkg, which performs several successive steps for each subject.
The first step was the registration of each subjects' brain MRI to a common space, using the subject's anatomical T1-weighted acquisition and the MNI (Montreal Neurological Institute) ICBM 2009c non-linear asymmetric template as a reference template. Registration was performed with the ANTS (Advanced Normalization Tools) toolbox, using a diffeomorphic transformation based on the Symmetric Normalization (SyN) approach [3].
The second step was the computation of the Diffusion Tensor Imaging (DTI) model [4] and the diffusion Orientation Distribution Functions (ODF) using the analytical Q-ball model [11] for each voxel of the brain.
The third step was the computation of a whole-brain tractogram from the ODF map, using a probabilistic algorithm [18] (tractography parameters are detailed in supplementary materials).
The fourth and final step was a dimensionality-reduction step, using an intra-subject clustering algorithm as described by Guevara et al [14], which groups the fibers together given their geometrical properties. White matter fibers were first separated in 4 different regions (left hemisphere, right hemisphere, inter-hemispheric and cerebellum) and grouped by length ranges. Fibers crossing through similar voxels are then clustered together using an average-link hierarchical clustering algorithm.

Group analysis and optic radiation analysis

After the tractography and intra-subject clustering were performed over the 1065 subjects, a cross-subject fiber clustering algorithm was applied to all the individual cluster centroid maps to establish maps of fascicles in common amongst the population, using the HDBscan algorithm [6] (algorithm parameters are detailed in supplementary materials).
The last step of the group analysis consisted of the identification of the optic radiations with a ROI selection strategy, using 2 ROIs drawn on the MNI template for each hemisphere: the first ROI corresponded to the delineation of the lateral geniculate nucleus, and the second ROI corresponded to a coronal area located in the occipital lobe, rostrally to the calcarine sulcus and the primary visual cortex. The resulting optical radiations were manually curated to remove residual artifactual fibers. The two final bundles obtained therefore constitute reference optic radiation bundles at the scale of the whole 1065 subjects' population. We then used these reference bundles to automatically label each subject's probabilistic tractography using a minimum pairwise distance algorithm and to finally reconstruct their individual optic radiations.

Distance of the individual left and right optical radiations to landmark points

Anatomical landmark points were placed on the MNI ICBM 2009c non-linear asymmetric anatomical T1-weighted MRI scan at the most rostral point of the temporal pole and the most rostral point of the temporal horn of the lateral ventricle for both sides by a trained neuro-anatomist. As each subject's brain MRI was previously

registered into the same MNI ICBM 2009c non-linear asymmetric anatomical T1-weighted template space, its optic radiations could therefore be projected into this space, in order to measure the distance between each of the individual optic radiations and those landmark points. The distance was positive if the anatomical point is located rostrally to the rostral ridge of the optic radiations, and negative if it is located caudally.

Results

Diffusion MRI processing

The dMRI post-processing pipeline, summarized in figure 1, was applied to each of the 1065 subjects. The probabilistic tractography resulted in a median number of 6 million fibers per subject, who were then classified in a median number of 215 000 fiber clusters (or fascicles) per subject.

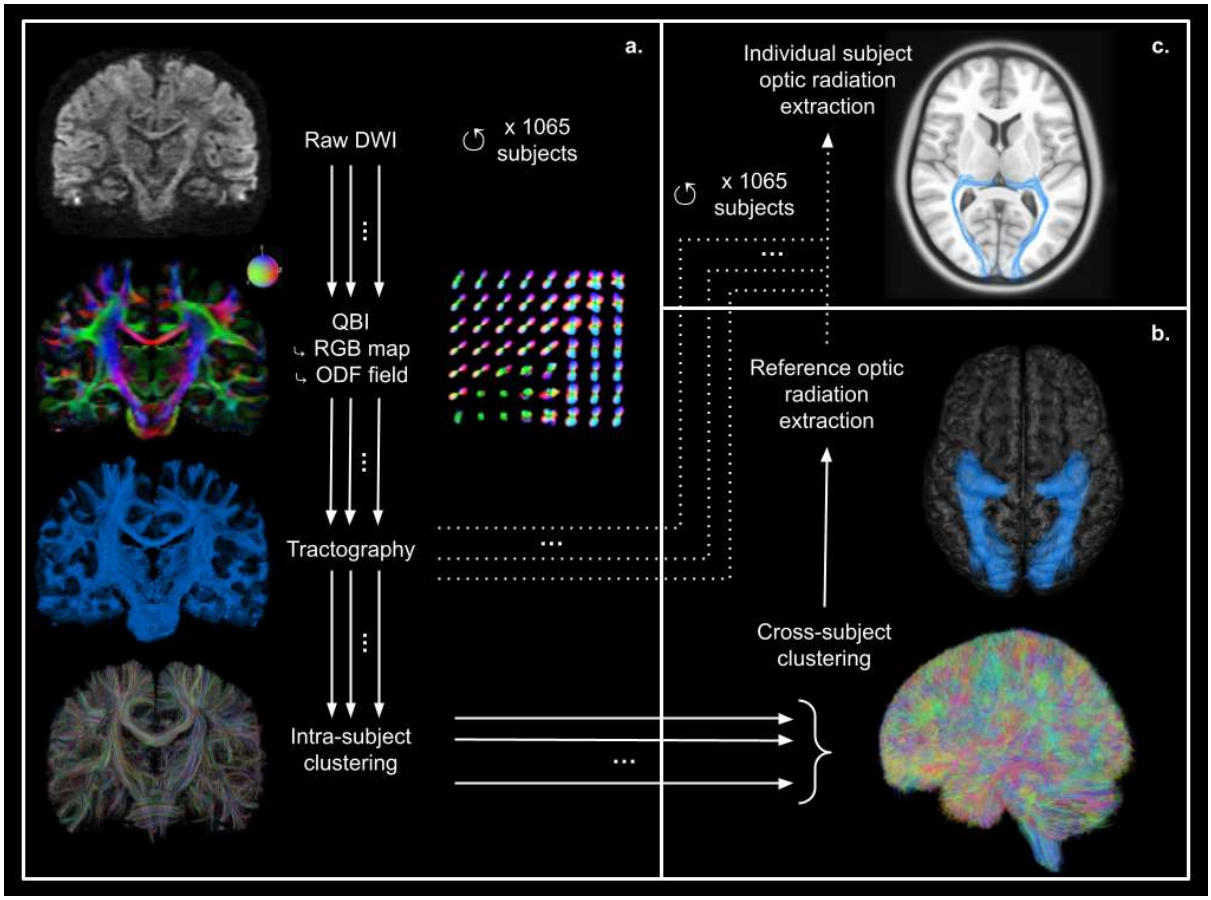

Figure 1. Overview of the complete dMRI analysis pipeline.
a: Individual dMRI analysis pipeline performed for each subject: from dMRI data, computation of the color-encoded RGB map showing the color-coded direction of main diffusivity (red = left-right; green = antero-posterior; blue = superior-inferior ; brightness is proportional to fractional anisotropy) and the ODF field for each voxel of the brain using the Q-Ball Imaging (QBI) model; computation of the whole-brain tractography; and intra-subject clustering where each color represents a fiber cluster.
b: Group analysis: cross-subject clustering on the whole 1065 subject's cluster maps, and extraction of a reference optic radiation bundle by ROI selection
c: Extraction of each subject's optic radiations, using a minimum pairwise algorithm between the reference optic radiation bundle and the subject's probabilistic tractography.

Group analysis was performed using the HDBscan algorithm in order to identify relevant fascicle clusters present in all subjects. The reference optic radiation bundles, resulting from the ROI selection strategy described previously, are shown in figure 2. These reference bundles were then applied to the individual probabilistic tractography of each subject to label fibers corresponding to the optic radiations, using a maximum pairwise distance algorithm. This algorithm successfully identified optic radiations in 100 % of the 1065 subjects, both for the left and right hemispheres.

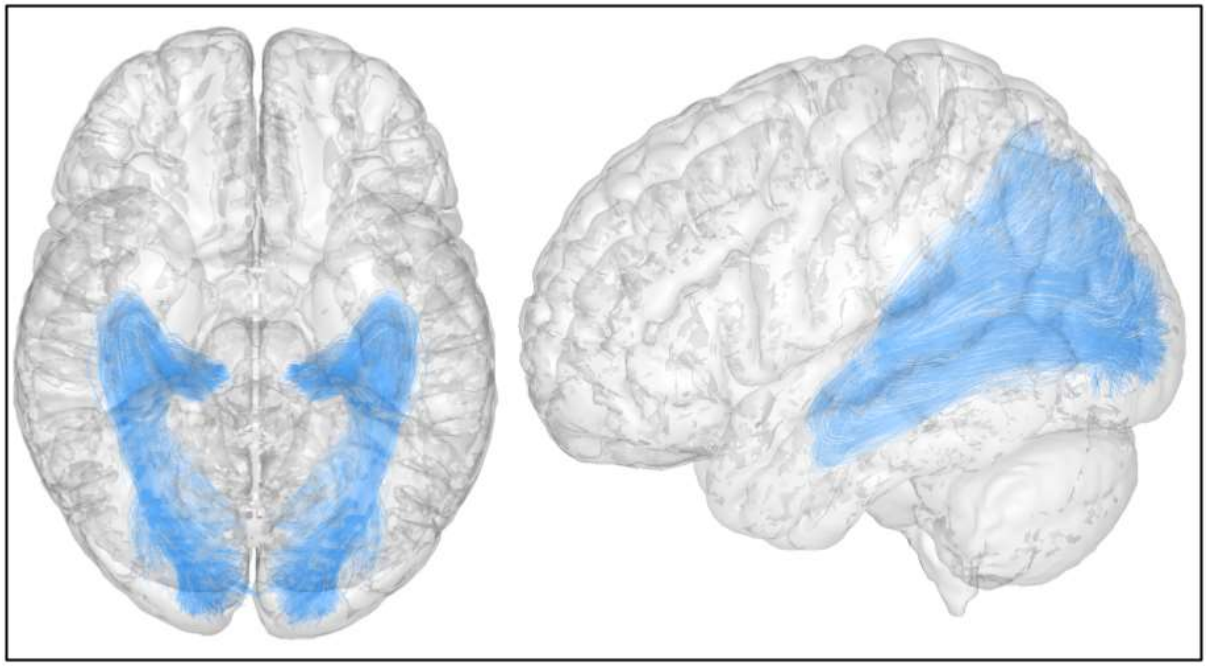

Figure 2. Reference optic radiation bundles, resulting from the inter-subject fiber clustering on the whole 1065 subjects cohort

Anatomical measurements

The rostral tip of the temporal pole (TP) and the rostral tip of the temporal horn (TH) of the lateral ventricle were defined for both hemispheres on the T1-weighted MNI ICBM 2009c non-linear asymmetric template (figure 3). The rostral tip of the optic radiation (OR) was automatically labeled for each subject, and the distance between TP and OR was measured for each subject on the sagittal plane.

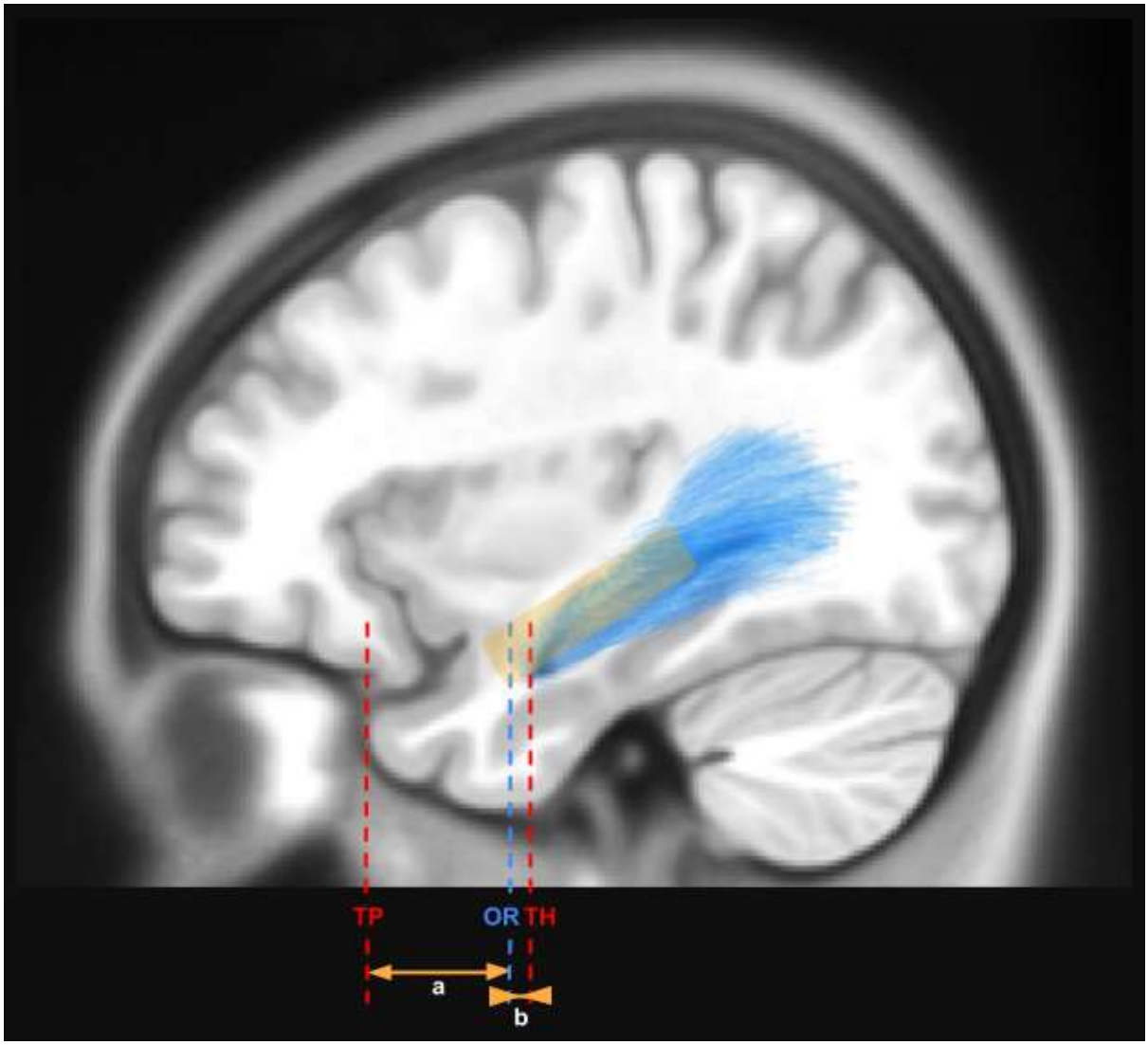

Figure 3. Anatomical measurement for each subject: distance (a) between the rostral ridge of the optic radiation (OR) and the rostral tip of the temporal pole (TP) and distance (b) between the rostral ridge of the optic radiation (OR) and the rostral tip of the temporal horn of the lateral ventricle (TH). The level of the temporal stem is displayed as an orange transparent box for anatomical landmarks.

At the population level, the median distance between the most rostral part of the optic radiation and the temporal pole was 28.8 mm (standard deviation SD: 2.3 mm ; mean: 28.7 mm ; range: 17.0 - 36.2 mm) for the left hemisphere and 29.2 mm (SD: 2.1 mm ; mean: 29.2 mm ; range: 20.6 - 35.8 mm) for the right hemisphere, as shown in figure 3.
The difference between both hemispheres was statistically significant ($p=1.10^{-8}$).

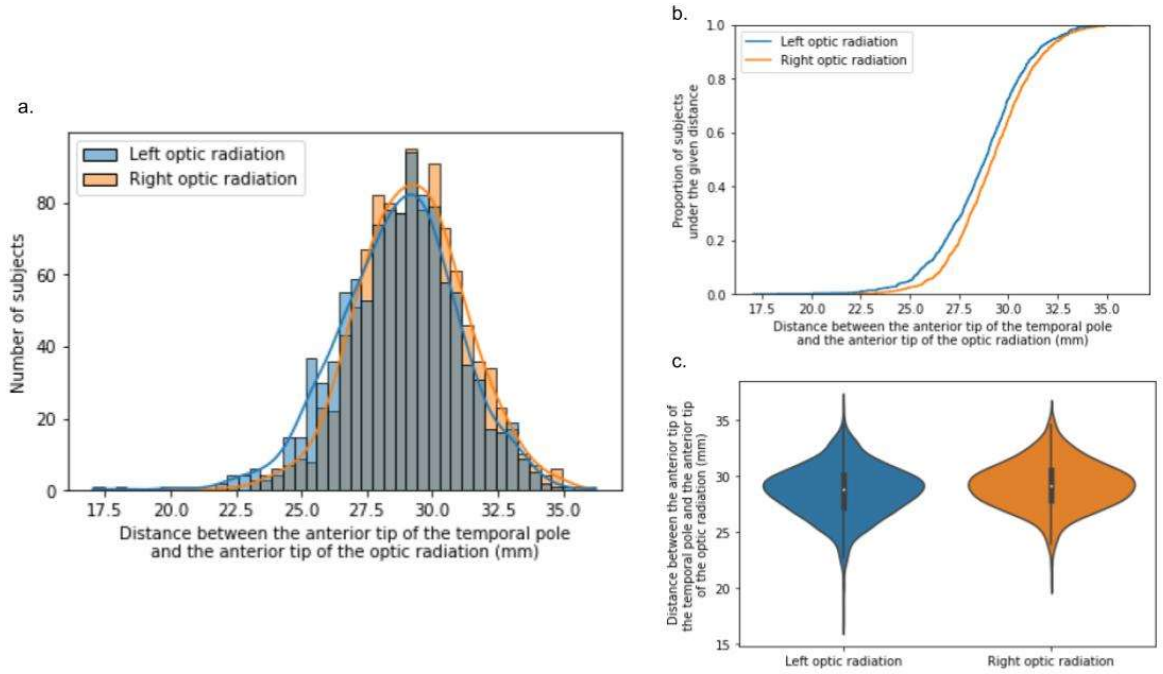

Figure 4. Distance measures between the rostral ridge of the optic radiations (OR) and the tip of the temporal pole (TP) across the whole population (1065 subjects). Blue: left side, orange: right side. a: histogram of the distance distribution across the population. b: cumulative distribution function (proportion of subjects falling below each unique distance value in the population) of the distance measure. c: violin plot of the distance distribution across the population (the inner box corresponds to the quartiles of the dataset, the central white dot represents the median value, and the bar extends to +/- 2 standard deviations)

The median distance between the tip of the optic radiation (OR) and the tip of the temporal horn (TP) was [-0.8 m] (SD: 2.1 mm) for the right hemisphere and [-1.2] mm (SD: 2.3 mm) for the left hemisphere ($p=1.10^{-8}$). The distance was negative if the optic radiation extends rostrally to the temporal horn, which was found in 771 subjects (72 %) for the left hemisphere, and 690 (65 %) subjects for the right hemisphere.

Discussion

To our knowledge, our study is carried out on the largest number of subjects presented in the literature, which enabled us to investigate in depth the anatomy and inter-subject variability of the optic radiations with a high level of accuracy. We confirmed a high inter-subject variability in the rostral extent of the optic radiation and a left-right physiological variability, which is of great importance for temporal lobe surgery.

Evolution of diffusion techniques

The first diffusion models used to assess the fiber directions, such as the Diffusion Tensor Imaging model [4], had many limitations, being unable (or hardly able) to assess fiber crossing from 2 or more different tracts inside a single voxel, or fiber bending or twisting of a given tract inside a voxel. More recent models known as High Angular Resolution Diffusion Imaging models (HARDI), such as Q-ball imaging [11], largely improved the quality of the local orientation estimations, being able to resolve multiple intra-voxel fiber orientations. Such models require more diffusion direction sampling, and/or acquisition at different b-values (multiple-shell acquisition), and therefore a longer acquisition time. Over the last decades, hardware and software progress in MRI systems as well as progress in the local modeling of the diffusion process made it possible to acquire such data in a reasonable amount of time, compatible with in-vivo acquisition in healthy subjects or in patients with neurological diseases.
To reconstruct fiber tracts, a simple and efficient tool is the deterministic streamline tractography algorithm [29], which builds the fibers starting from seeds placed in each voxel and reconstructs a fiber step by step, following the direction of highest diffusivity within each voxel. Despite the use of regularization schemes to avoid the creation of false positives (eg artifactual trajectories), this deterministic approach remains highly sensitive to any error present in the ODF map induced by various sources of artifacts (presence of physical noise, presence of residual geometrical distortions, limitations of the biophysical model, …). An alternative solution relies on the use of probabilistic tractography approaches [18], iteratively generating multiple streamlines, based on a probability distribution of diffusion orientation instead of a single orientation, and modeling multiple diffusion orientations per voxel by randomly sampling a direction around the main diffusion direction.
White matter tractography from diffusion MRI has been assessed for years, and has demonstrated to be reliable to study the white matter tracts connecting the occipital cortex [1, 7, 19, 25]. Probabilistic tractography techniques have proven to be more reliable than deterministic tractography techniques to study the complex optic radiation anatomy [20], with a better match with dissection studies [9]. We therefore chose to use this method.

Comparison to post-mortem studies

In our cohort**,** the median distance between the most rostral part of the optic radiation and the temporal pole was 29.2 mm (standard deviation SD: 2.1 mm) for the right hemisphere and 28.8 mm (SD: 2.3 mm) for the left hemisphere. This is compatible with results found by post-mortem studies: in a brain dissection study performed in 20 subjects [26], the distance between the rostral edge of the optic radiations and the temporal pole ranged between 20 and 33 mm (mean: 28.4 mm), and the optic radiations extended rostrally to the temporal horn in all subjects with a mean distance of [-4.7 mm] (range: [-2] to [-7] mm). In the largest existing post-mortem study in 25 subjects [13], the mean distance between the temporal pole and the tip of the optical radiations was found to be 27 mm (SD: 3.5 mm), and the mean distance between the tip of the temporal horn and the tip of the optical radiations was found to be [-5 mm] (SD: 3.9 mm). A few other studies, summarized in table 1, performed on smaller numbers of subjects [30, 31] also found similar results and highlighted the interindividual variability.

Comparison to existing diffusion MRI tractography studies

Prior brain dMRI tractography studies that measured the rostral extent of the optic radiations found different results depending on the hardware and method used, which highlights the importance of using up-to-date diffusion and tractography methods. In a cohort of 9 subjects (7 healthy subjects and 2 patients with temporal

resection) [24] using a 1.5T MRI scanner and a deterministic tractography algorithm, the distance from the most rostral part of the optic radiations to the temporal pole ranged from 34 to 51 mm (mean: 44 mm), which is significantly higher than the results of post-mortem dissection studies. In another MRI study [41] of 41 subjects (20 healthy subjects and 21 patients with temporal resection) using a 3T MRI scanner and a probabilistic tractography technique, closer but still different results were found: the distance between the tip of the temporal pole and the tip of the optic radiations ranged from 24 to 43 mm (mean: 34 mm), and the distance from the tip of Meyer's loop to the temporal horn ranged from -15 to +9 mm (mean: 0 mm). The authors also performed a multiple regression analysis, showing that the distance between the temporal pole and the tip of Meyer's loop was an independent predictor of postoperative visual field defect (β = -0.80). Finally, in a study [32] of 30 healthy subjects using a 3T MRI scanner and a probabilistic tractography technique, the mean distance between the rostral ridge of optic radiations and the tip of the temporal pole was 23.1 mm in the left hemisphere, and 26.41 mm in the right hemisphere, more in line with the dissection studies and ours. The results of those studies, as well as a few other tractography studies [8, 33, 36, 40], are summarized in table 1.
With our methodology combining a large number of individuals, a high-resolution angular and spatial diffusion MRI dataset and a state-of-the-art diffusion analysis methodology, we found a better agreement with histological data, demonstrating the reliability of such *in vivo* studies.

Article	**Type of study**	**MRI scanner hardware and tractography algorithm**	**Number of subjects**	**Distance between the tip of the temporal pole and the tip of the optic radiations**
Ebeling et Reulen, 1988 [13]	Dissection	n.a.	25 subjects (50 hemisphere)	Mean: 27 mm (SD: +/- 3.5 mm)
Peuskens et al, 2004 [30]	Dissection	n.a.	17 hemispheres	Mean: not reported (range: 15 to 30 mm)
Rubino et al, 2005 [31]	Dissection	n.a.	20 hemispheres	Mean: 25 mm (range: 22 to 30 mm)
Parraga et al, 2012 [26]	Dissection	n.a.	20 subjects (40 hemispheres)	Mean: 28.4 mm (range: 20 to 33 mm)
Yamamoto et al, 2005 [40]	Diffusion MRI tractography	1.5 T MRI Deterministic	5 healthy subjects	Mean: 37.3 mm (range: 33.1 to 40.0 mm)
Nilsson et al, 2007 [24]	Diffusion MRI tractography	1.5 T MRI Deterministic	9 subjects (2 patients and 7 healthy subjects)	Mean: 44mm (range: 34 to 51 mm)
Taoka et al, 2008 [36]	Diffusion MRI tractography	1.5 T MRI Deterministic	14 patients	Mean: 36.6 mm (range: 30.0 to 43.2 mm)
Sherbondy et al, 2008 [33]	Diffusion MRI tractography	1.5 T MRI Probabilistic	8 healthy subjects	Mean: 28 mm (SD: +/- 3 mm)

Yogarajah et al, 2009 [41]	Diffusion MRI tractography	3 T MRI Probabilistic	41 subjects (21 patients and 20 healthy subjects)	*Healthy subjects:* Mean: 35 mm (range: 24 to 47 mm) *Patients:* Mean: 34 mm (range: 24 to 43 mm)
Chen et al, 2009 [8]	Diffusion MRI tractography	1.5 T MRI Deterministic	48 patients	Mean: 32.1 mm (range: 20.9 to 51.5 mm)
Lilja et al, 2014 [20]	Diffusion MRI tractography	1.5 T MRI Deterministic and probabilistic	23 subjects (11 healthy subjects, 5 pre-surgical and 7 post-surgical patients)	*Deterministic:* Mean: 44 mm (range: 34 to 51 mm) *Probabilistic:* Mean: 33 mm (range: 25 to 48 mm)
James et al, 2015 [15]	Diffusion MRI tractography	1.5 T MRI Probabilistic	100 subjects (75 healthy subjects and 25 patients)	*Left side:* Mean: 37.44 mm (range: 32.2 to 46.6 mm) *Right side:* Mean: 39.08 mm (range: 34.3 to 49.7 mm)
Shan et al, 2019 [32]	Diffusion MRI tractography	3 T MRI Probabilistic	30 healthy subjects	*Left side:* Mean: 23.1 mm *Right side:* Mean: 26.41 mm
Ours	Diffusion MRI tractography	3T MRI Probabilistic	1065 healthy subjects	*Left side:* Mean: 28.7 mm (range: 17.0 to 36.2 mm) *Right side:* Mean: 29.2 mm (range: 20.6 to 35.8 mm)

Left-right anatomical variability

In our cohort, the median distance between the tip of the temporal pole and the rostral extent of the optic radiation was 29.2 mm for the right side and 28.8 mm for the left side, with a statistically significant difference between both hemispheres ($p=1.10^{-8}$). We found a higher number of subjects under any given distance threshold ranging from 24 to 32mm on the left side. A few other studies have already reported slight left-right differences. A study in 25 patients and 75 healthy subjects [15] using a 1.5 T MRI scanner and a probabilistic tractography algorithm found that the distance from the rostral part of the optic radiations to the temporal pole was 37.44 +/- 4.7 mm for the left side and 39.08 +/- 4.9 mm for the right side. A left-right difference was also found in another study in 20 healthy subjects [12], with shorter left distances between the tip of the optic radiation and the temporal pole (23.1 mm for the left side and 26.41 mm for the right side). The more extreme value depicted in the left side in our study may explain the higher risk of postoperative visual defect after left-sided temporal brain surgeries [16], underlying the importance of performing anatomical studies of variability from large cohorts.

Comparison with the arcuate fasciculus

The main tract for which interhemispheric asymmetry has been studied is the arcuate fasciculus, both in dissection and MRI studies. This fasciculus exhibits a great left-right asymmetry, which is not really surprising

due to its implication in the langage network. In dissection studies, the arcuate fasciculus therefore has a wider coronal section on the left side than on the right side (95 +/- 21 mm vs 59 +/- 12 mm) [17], which indicates a higher number of fibers. Moreover, its cortical connections are more extensive on the left side. In particular, the left arcuate fasciculus extends further than the right in the frontal and temporal lobe [37], and its connections from the left Broca's area to the left temporal lobe are much more dense and extensive than their right-side counterpart [35]. One might hypothesize that, as the arcuate fasciculus is larger on the left side, this could lead to modifications in the anatomical pathways of other tracts in the same hemisphere, which may explain the differences observed in the optic radiation anatomy. This strong anatomical asymmetry of the arcuate fasciculus was explained by the role of the left arcuate fasciculus in the language network, and has been linked in other studies with language performances, but not with handedness [2]. In the HCP cohort, the handedness was assessed with a Handedness Laterality Score, ranging from -100 (left) to +100 (right-handedness preference), and we observed no difference in optic radiation anatomy according to the laterality.

Application to neurosurgical planning

The risk of optic radiation injury is high in mesial temporal lobe surgery, even with current conservative resection methods [16, 22, 27]. Moreover, this risk is also present for certain surgical approaches : the temporal T1-T2 trans-sulcal approach has become a standard approach for resection of intraventricular tumors of the temporal horn [21], and is widely used for resection of glial tumors of the temporal area [23]. Trans-sulcal approach reduces the risk of fascicular injury compared to other approaches, but does not eliminate it, and the knowledge gained from this study about the anatomical variability of the optic radiation and their inter-hemispheric asymmetry would also be useful for this kind of surgical approach.

The optic radiation atlas we developed from an inter-subject fiber clustering approach on the whole 1065 subjects HCP cohort was efficiently used to extract optic radiations on an individual scale. Its extension to the extraction of optic radiations of any other subject is straightforward and consists of 3 simple steps: 1) matching the new subject's T1w anatomy to the MNI ICBM152 template space; 2) reconstructing the whole brain connectogram of the subject from any HARDI dMRI dataset using a probabilistic fiber tracking approach; 3) applying our novel MNI-based optical radiation bundle atlas to identify the fibers belonging to optic radiations. Both the MNI-based optical radiation bundle atlas and corresponding post-processing pipeline are freely available from the Ginkgo toolbox GitLab repository accessible at https://framagit.org/cpoupon/gkg.

Limitations of the study

The main limitation of our study is the absence of histological data on the HCP cohort. We therefore lack a direct comparison between the fiber bundles reconstructed from dMRI tractography and from Klinger's dissections. However, previous studies [9, 10, 20] using the same diffusion methodology have compared histological data and probabilistic tractography and found a good agreement between the two *in* and *ex vivo* approaches, and our own results are in accordance with published histological data.

Conclusion

We demonstrated *in vivo* the presence of a significant inter-subject variability of the optic radiations from the population of 1065 healthy volunteers stemming from the Human Connectome Project, notably for two parameters: the rostral extension of these radiations and the left-right asymmetry. We built a novel dMRI-based optic radiation bundle atlas that can be used for fast optic radiation reconstruction from any dMRI tractography in order to identify subjects at higher risk of visual field defect after temporal surgery and individually guide the neurosurgical procedure. These results highlight the importance of performing individual dMRI tractography with appropriate methodology before neurosurgery.

Declarations

Ethical Approval

This research was performed on the Wu-Minn HCP Database, an open-access MRI database available at https://www.humanconnectome.org/. Subjects included had given their written consent to the Wu-Minn Consortium for their data to be published in open-access and reused for other studies. All authors approved the DataUse Terms from the Wu-Minn HCP Consortium, a guideline for accessing, using and performing analyses on this open-access database.

We followed the French ethical guidelines and the current French legislation, i.e. : The World Medical Association Declaration of Helsinki Ethical Principles for Medical Research Involving Human Subjects (https://www.wma.net/wp-content/uploads/2016/11/DoH-Oct2013-JAMA.pdf) and the French Public Health Law n°2004-806 (https://www.legifrance.gouv.fr/jorf/id/JORFTEXT000000787078/)

Competing interests

The authors declare no competing interest

Authors' contributions

B. Herlin: Protocol/project development, Data collection or management, Data analysis, Manuscript writing
I. Uszynski: Protocol/project development, Data management, Data Analysis, Manuscript writing/editing
M. Chauvel: Protocol/project development, Data analysis
C. Poupon : Protocol/project development, Manuscript writing/editing
S. Dupont: Protocol/project development, Manuscript writing/editing

Funding

This research has received funding from the European Union's Horizon 2020 Framework Program for Research and Innovation under the specific Grant No. 945539 (Human Brain Project SGA3).

Availability of data and materials

This research was performed on the Wu-Minn HCP Database, an open-access MRI database available at https://www.humanconnectome.org/.

All analyses were performed using the Ginkgo toolbox developed by the CEA/NeuroSpin team and freely available at https://framagit.org/cpoupon/gkg

Supplementary materials

Supplementary material 1. Information on data acquisition and diffusion pipeline parameters

MRI acquisitions were conducted on a Connectome Skyra 3T MRI scanner. The T1w acquisition was performed using a 3D MPRAGE sequence, with a 0.7mm isotropic spatial resolution and a TR/TE = 2400/2.14 ms. The dMRI acquisitions were performed using a 2D monopolar pulsed-gradient-spin-echo (PGSE) single-shot multiband EPI sequence, with a multi-band factor of 3, a 1.25mm isotropic spatial resolution, a TR/TE = 5520/89.50 ms, and a multiple shell sampling of the q-space relying on 3 b-values of 1000, 2000, and 3000 s/mm2 with 90 uniformly distributed diffusion directions per shell, plus 6 non diffusion-weighted b=0s/mm² reference images
The parameters used for the probabilistic tractography algorithm were : 8 seeds per voxel over a predefined domain of propagation computed from the averaged b=0s/mm² image, aperture angle of 30°, fiber length range of 1.25 – 300 mm, forward and backward integration step of 0.3 mm, temperature of the Gibb's sampler of 1. The fiber length range enabled discarding fibers smaller than the voxel size (minimum length range) and to prevent the existence of infinite loops
The parameters used for the HDBscan were : normalization factor 6, neighbor count 5, minimum cluster size 10, minimum subject percentage 2.5 %. Those parameters were optimized by a grid search on the database to maximize the number of clusters.

References:

1. Abed Rabbo F, Koch G, Lefèvre C, Seizeur R (2018) Stereoscopic visual area connectivity: a diffusion tensor imaging study. Surg Radiol Anat 40:1197–1208. doi: 10.1007/s00276-018-2076-3
2. Allendorfer JB, Hernando KA, Hossain S, Nenert R, Holland SK, Szaflarski JP (2016) Arcuate fasciculus asymmetry has a hand in language function but not handedness. Hum Brain Mapp 37:3297–3309. doi: 10.1002/hbm.23241
3. Avants BB, Epstein CL, Grossman M, Gee JC (2008) Symmetric diffeomorphic image registration with cross-correlation: evaluating automated labeling of elderly and neurodegenerative brain. Med Image Anal 12:26–41. doi: 10.1016/j.media.2007.06.004
4. Basser PJ, Mattiello J, LeBihan D (1994) MR diffusion tensor spectroscopy and imaging. Biophys J 66:259–267. doi: 10.1016/S0006-3495(94)80775-1
5. Bürgel U, Schormann T, Schleicher A, Zilles K (1999) Mapping of Histologically Identified Long Fiber Tracts in Human Cerebral Hemispheres to the MRI Volume of a Reference Brain: Position and Spatial Variability of the Optic Radiation. NeuroImage 10:489–499. doi: 10.1006/nimg.1999.0497
6. Campello RJGB, Moulavi D, Sander J (2013) Density-Based Clustering Based on Hierarchical Density Estimates. In: Pei J, Tseng VS, Cao L, Motoda H, Xu G (eds) Advances in Knowledge Discovery and Data Mining. Springer, Berlin, Heidelberg, pp 160–172
7. Catani M, Jones DK, Donato R, ffytche DH (2003) Occipito-temporal connections in the human brain. Brain 126:2093–2107. doi: 10.1093/brain/awg203
8. Chen X, Weigel D, Ganslandt O, Buchfelder M, Nimsky C (2009) Prediction of visual field deficits by diffusion tensor imaging in temporal lobe epilepsy surgery. NeuroImage 45:286–297. doi: 10.1016/j.neuroimage.2008.11.038
9. Clatworthy PL, Williams GB, Acosta-Cabronero J, Jones SP, Harding SG, Johansen-Berg H, Baron J-C (2010) Probabilistic tractography of the optic radiations--an automated method and anatomical validation. NeuroImage 49:2001–2012. doi: 10.1016/j.neuroimage.2009.10.083
10. Dayan M, Kreutzer S, Clark CA (2015) Tractography of the optic radiation: a repeatability and reproducibility study. NMR Biomed 28:423–431. doi: 10.1002/nbm.3266
11. Descoteaux M, Angelino E, Fitzgibbons S, Deriche R (2007) Regularized, fast, and robust analytical Q-ball imaging. Magn Reson Med 58:497–510. doi: 10.1002/mrm.21277
12. Dreessen de Gervai P, Sboto-Frankenstein UN, Bolster RB, Thind S, Gruwel MLH, Smith SD, Tomanek B (2014) Tractography of Meyer's Loop asymmetries. Epilepsy Res 108:872–882. doi: 10.1016/j.eplepsyres.2014.03.006
13. Ebeling U, Reulen H-J (1988) Neurosurgical topography of the optic radiation in the temporal lobe. Acta Neurochir (Wien) 92:29–36. doi: 10.1007/BF01401969
14. Guevara P, Poupon C, Rivière D, Cointepas Y, Marrakchi-Kacem L, Descoteaux M, Fillard P, Thirion B, Mangin J-F (2010) Inference of a HARDI fiber bundle atlas using a two-level clustering strategy. Med Image Comput Comput-Assist Interv MICCAI Int Conf Med Image Comput Comput-Assist Interv 13:550–7
15. James JS, Radhakrishnan A, Thomas B, Madhusoodanan M, Kesavadas C, Abraham M, Menon R, Rathore C, Vilanilam G (2015) Diffusion tensor imaging tractography of Meyer's loop in planning resective surgery for drug-resistant temporal lobe epilepsy. Epilepsy Res 110:95–104. doi: 10.1016/j.eplepsyres.2014.11.020
16. Jeelani NUO, Jindahra P, Tamber MS, Poon TL, Kabasele P, James-Galton M, Stevens J, Duncan J, McEvoy AW, Harkness W, Plant GT (2010) "Hemispherical asymmetry in the Meyer's Loop": a prospective study of visual-field deficits in 105 cases undergoing anterior temporal lobe resection for epilepsy. J Neurol Neurosurg Psychiatry 81:985–991. doi: 10.1136/jnnp.2009.182378
17. de Jong L, Kovacs S, Bamps S, Van Calenbergh F, Sunaert S, van Loon J (2009) The arcuate fasciculus: a comparison between diffusion tensor tractography and anatomy using the fiber dissection technique. Surg Neurol 71:153. doi: 10.1016/j.surneu.2008.10.072
18. Koch MA, Norris DG, Hund-Georgiadis M (2002) An Investigation of Functional and Anatomical Connectivity Using Magnetic Resonance Imaging. NeuroImage 16:241–250. doi: 10.1006/nimg.2001.1052
19. Lavrador JP, Ferreira V, Lourenço M, Alexandre I, Rocha M, Oliveira E, Kailaya-Vasan A, Neto L (2019) White-matter commissures: a clinically focused anatomical review. Surg Radiol Anat 41:613–624. doi: 10.1007/s00276-019-02218-7
20. Lilja Y, Ljungberg M, Starck G, Malmgren K, Rydenhag B, Nilsson DT (2014) Visualizing Meyer's loop: A comparison of deterministic and probabilistic tractography. Epilepsy Res 108:481–490. doi: 10.1016/j.eplepsyres.2014.01.017
21. Ma J, Cheng L, Wang G, Lin S (2014) Surgical management of meningioma of the trigone area of the

lateral ventricle. World Neurosurg 82:757–769. doi: 10.1016/j.wneu.2014.05.026
22. Manji H, Plant G (2000) Epilepsy surgery, visual fields, and driving: a study of the visual field criteria for driving in patients after temporal lobe epilepsy surgery with a comparison of Goldmann and Esterman perimetry. J Neurol Neurosurg Psychiatry 68:80–82. doi: 10.1136/jnnp.68.1.80
23. Monroy-Sosa A, Navarro-Fernández JO, Chakravarthi SS, Rodríguez-Orozco J, Rovin R, de la Garza J, Kassam A (2021) Minimally invasive trans-sulcal parafascicular surgical resection of cerebral tumors: translating anatomy to early clinical experience. Neurosurg Rev 44:1611–1624. doi: 10.1007/s10143-020-01349-5
24. Nilsson D, Starck G, Ljungberg M, Ribbelin S, Jönsson L, Malmgren K, Rydenhag B (2007) Intersubject variability in the anterior extent of the optic radiation assessed by tractography. Epilepsy Res 77:11–16. doi: 10.1016/j.eplepsyres.2007.07.012
25. Palejwala AH, O'Connor KP, Pelargos P, Briggs RG, Milton CK, Conner AK, Milligan TM, O'Donoghue DL, Glenn CA, Sughrue ME (2020) Anatomy and white matter connections of the lateral occipital cortex. Surg Radiol Anat 42:315–328. doi: 10.1007/s00276-019-02371-z
26. Párraga RG, Ribas GC, Welling LC, Alves RV, de Oliveira E (2012) Microsurgical anatomy of the optic radiation and related fibers in 3-dimensional images. Neurosurgery 71:160–171; discussion 171-172. doi: 10.1227/NEU.0b013e3182556fde
27. Pathak-Ray V, Ray A, Walters R, Hatfield R (2002) Detection of visual field defects in patients after anterior temporal lobectomy for mesial temporal sclerosis-establishing eligibility to drive. Eye Lond Engl 16:744–748. doi: 10.1038/sj.eye.6700152
28. Peltier J, Travers N, Destrieux C, Velut S (2006) Optic radiations: a microsurgical anatomical study. J Neurosurg 105:294–300. doi: 10.3171/jns.2006.105.2.294
29. Perrin M, Poupon C, Cointepas Y, Rieul B, Golestani N, Pallier C, Rivière D, Constantinesco A, Le Bihan D, Mangin JF (2005) Fiber tracking in q-ball fields using regularized particle trajectories. Inf Process Med Imaging Proc Conf 19:52–63. doi: 10.1007/11505730_5
30. Peuskens D, van Loon J, Van Calenbergh F, van den Bergh R, Goffin J, Plets C (2004) Anatomy of the anterior temporal lobe and the frontotemporal region demonstrated by fiber dissection. Neurosurgery 55:1174–1184. doi: 10.1227/01.neu.0000140843.62311.24
31. Rubino PA, Rhoton AL, Tong X, Oliveira E de (2005) Three-dimensional relationships of the optic radiation. Neurosurgery 57:219–227; discussion 219-227. doi: 10.1227/01.neu.0000176415.83417.16
32. Shan Y-Z, Wang Z-M, Fan X-T, Zhang H-Q, Ren L-K, Wei P-H, Zhao G-G (2019) Automatic labeling of the fanning and curving shape of Meyer's loop for epilepsy surgery: an atlas extracted from high-definition fiber tractography. BMC Neurol 19:302. doi: 10.1186/s12883-019-1537-6
33. Sherbondy AJ, Dougherty RF, Napel S, Wandell BA (2008) Identifying the human optic radiation using diffusion imaging and fiber tractography. J Vis 8:12. doi: 10.1167/8.10.12
34. Sivakanthan S, Neal E, Murtagh R, Vale FL (2016) The evolving utility of diffusion tensor tractography in the surgical management of temporal lobe epilepsy: a review. Acta Neurochir (Wien) 158:2185–2193. doi: 10.1007/s00701-016-2910-5
35. Takaya S, Kuperberg GR, Liu H, Greve DN, Makris N, Stufflebeam SM (2015) Asymmetric projections of the arcuate fasciculus to the temporal cortex underlie lateralized language function in the human brain. Front Neuroanat 9:119. doi: 10.3389/fnana.2015.00119
36. Taoka T, Sakamoto M, Nakagawa H, Nakase H, Iwasaki S, Takayama K, Taoka K, Hoshida T, Sakaki T, Kichikawa K (2008) Diffusion tensor tractography of the Meyer loop in cases of temporal lobe resection for temporal lobe epilepsy: correlation between postsurgical visual field defect and anterior limit of Meyer loop on tractography. AJNR Am J Neuroradiol 29:1329–1334. doi: 10.3174/ajnr.A1101
37. Thiebaut de Schotten M, Ffytche DH, Bizzi A, Dell'Acqua F, Allin M, Walshe M, Murray R, Williams SC, Murphy DGM, Catani M (2011) Atlasing location, asymmetry and inter-subject variability of white matter tracts in the human brain with MR diffusion tractography. NeuroImage 54:49–59. doi: 10.1016/j.neuroimage.2010.07.055
38. Thudium MO, Campos AR, Urbach H, Clusmann H (2010) The basal temporal approach for mesial temporal surgery: sparing the Meyer loop with navigated diffusion tensor tractography. Neurosurgery 67:385–390. doi: 10.1227/NEU.0b013e3181f7424b
39. Van Essen DC, Smith SM, Barch DM, Behrens TEJ, Yacoub E, Ugurbil K, WU-Minn HCP Consortium (2013) The WU-Minn Human Connectome Project: an overview. NeuroImage 80:62–79. doi: 10.1016/j.neuroimage.2013.05.041
40. Yamamoto T, Yamada K, Nishimura T, Kinoshita S (2005) Tractography to Depict Three Layers of Visual Field Trajectories to the Calcarine Gyri. Am J Ophthalmol 140:781-785.e1. doi: 10.1016/j.ajo.2005.05.018
41. Yogarajah M, Focke NK, Bonelli S, Cercignani M, Acheson J, Parker GJM, Alexander DC, McEvoy AW, Symms MR, Koepp MJ, Duncan JS (2009) Defining Meyer's loop-temporal lobe resections, visual

field deficits and diffusion tensor tractography. Brain J Neurol 132:1656–1668. doi: 10.1093/brain/awp114